THE JOURNAL OF PHYSICAL CHEMISTRY C

Article

pubs.acs.org/JPCC

Energy Accommodation between Noble Gases and Carbon Nanotubes

Lin Hu and Alan J. H. McGaughey*

Department of Mechanical Engineering, Carnegie Mellon University, Pittsburgh, Pennsylvania 15213, United States

ABSTRACT: Molecular dynamics simulations are used to predict the energy accommodation coefficients (EACs) between the noble gases He, Ne, and Ar and the outside of single-walled carbon nanotubes (CNTs) with diameters between 0.41 and 6.10 nm at a temperature of 300 K. The EAC increases monotonically with CNT diameter and approaches the value predicted for graphene. The EAC also increases monotonically with gas atom mass. The CNT EAC data collapse to a linear trend when they are normalized by the graphene EAC and plotted versus the depth of their potential energy well on the CNT normalized by that for graphene. The EACs are used to estimate that the thermal boundary conductance between noble gases and graphene will be of order 0.1 MW/m^2·K at a gas pressure of 1 atm, corresponding to a gas Kapitza length of order 100 nm.

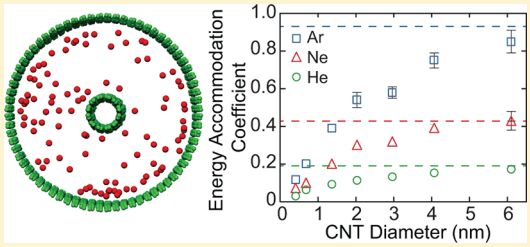

INTRODUCTION

The unique structure and properties of carbon nanotubes (CNTs) have led to their use in electronics, energy storage, and energy conversion devices. When using CNTs as gas sensors,[1,2] vertically arrayed film coatings to enhance heat removal,[3] hydrogen-storage materials,[4,5] or field emitters,[6,7] they are surrounded by and/or filled with gas molecules. Due to a CNT's large surface-area-to-volume ratio, the dynamics of the energy exchange between the gas molecules and the CNT will affect device performance or, in the case of a gas sensor, lead to its sensitivity. It is also important to include the effects of a gaseous environment when interpreting experimental measurements of CNT thermal conductivity.[8]

The extent of thermal acclimation between a solid and a gas is characterized by the energy accommodation coefficient (EAC), α, defined as[9]

$$\alpha = \frac{E_{\text{incident}} - E_{\text{reflected}}}{E_{\text{incident}} - E_{\text{solid}}} \quad (1)$$

Here, E_{incident} and $E_{\text{reflected}}$ are the gas energy flows incident to and reflected from the solid and E_{solid} is the reflected gas energy flow if the gas molecules had the same temperature as the solid. There is also a momentum accommodation coefficient, which can be used to describe rarefied gas flows adjacent to a solid (e.g., gas flow inside a CNT[10] or a nanochannel[11]).

Gas−surface interactions and the EAC depend on the depth of the potential energy well for the gas atom−surface interaction and the mass ratio between the gas and surface atoms,[12−15] and they can be controlled by modifying the surface stiffness through the addition of a self-assembled monolayer.[16−19] From the EAC, one can calculate the thermal boundary conductance,[20] needed to predict the rate of heat transfer between the gas and the surface. This parameter is of critical importance in designing thermal management strategies in micro- and nanosystems.[21]

We will focus on the EAC of the noble gases He, Ne, and Ar on the outside of a CNT. Due to the small size of a CNT, it is difficult to directly measure the EAC. Using molecular beam scattering (MBS), where gas molecules are launched at a surface over a range of incident angles, Kinefuchi et al. measured the EAC of He interacting with a vertically aligned array of bundled single-walled CNTs to be 0.76 (0.1 μm CNTs) and 0.97 (4 μm CNTs) at a temperature of 300 K.[3] Schiffres et al. studied the energy exchange between gas molecules (H_2, He, Ne, N_2, Ar) and single-walled CNTs at room temperature by measuring the thermal conductivity of a gas-permeated low-density CNT network (average CNT diameter of 0.9 nm). They found gas energy travel distances of 1−5 μm that increased with decreasing EAC.[22] Both of these measurements capture the cumulative effect of multiple gas−CNT collisions and do not provide information about individual collisions.

Molecular dynamics (MD) simulations can be used to investigate the atomistic dynamics of gas molecules interacting with solid surfaces. Two methods have been proposed. The first mimics the MBS experiment by considering individual gas molecule−solid collisions.[23] The second uses a nonequilibrium steady-state MD simulation where an ensemble of gas molecules interact with a solid source and sink.[22,24] In both methods, the EAC is calculated by monitoring the energy change of the gas molecules during collisions with the solid. The MBS method has a short simulation time for each collision but requires a large number of samples to represent the different collision conditions. It is crucial to properly set the incident velocity and angle distributions in this method.[11] The nonequilibrium MD method allows the gas dynamics to naturally evolve over one long simulation, capturing many

Received: April 26, 2013
Revised: August 19, 2013
Published: August 22, 2013

collisions, and is insensitive to the initial conditions once steady-state is reached.

The majority of previous MD studies of gas−graphitic surface thermal interactions used the MBS method. Någård et al. studied the collisions of Xe atoms with graphite,[25] and Bolton and co-workers studied the collisions of H_2, He, C, Ne, and Xe on a (10,0) CNT,[26,27] but neither report EACs. Kovalev et al. predicted the EAC of H_2 on graphite for gas and solid temperatures ranging between 77 and 1120 K.[28] Daun et al. predicted the EACs of He, Ne, Ar, Kr, and Xe at a temperature of 300 K on graphite at 3000 K to range from 0.19 (He) to 0.47 (Xe).[29]

CALCULATION METHODOLOGY

In this study, we extend the nonequilibrium MD method work presented in Schiffres et al.[22] to predict the diameter-dependence of the EAC of the noble gases He, Ne, and Ar on the outside of CNTs. Our focus is on systems near a temperature of 300 K, such that the gas atoms have low translational energies compared to typical MBS experiments. The simulation setup is shown in Figure 1 and comprises two concentric single-walled CNTs of 50 nm length with a periodic boundary condition applied along their axes. The inner CNT diameter ranges from 0.41 to 6.10 nm [chirality vectors ranging from (3,3) to (45,45)]. The outer CNT has a diameter of 8 nm [chirality vector of (60,60)] for inner CNT diameters less than 6 nm, and 10 nm [chirality vector of (75,75)] when the inner CNT diameter is 6 nm. The EAC on graphene (i.e., a CNT with infinite diameter) was also calculated by confining gas atoms between two graphene layers of size 5 nm by 50 nm separated by 40 nm. Periodic boundary conditions are applied in the plane of the layers. The number of carbon atoms ranges from 40,000 to 100,000. The number of gas atoms ranges from 250 to 800, corresponding to a pressure of 10 atm. This high pressure reduces the simulation time by tracking more gas atoms simultaneously. The resulting gas velocity distribution is Maxwell−Boltzmann, indicating that the outer CNT does not influence the predictions.

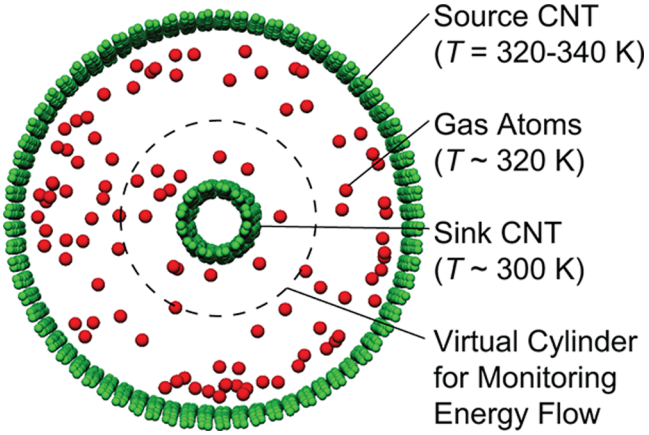

Figure 1. Molecular dynamics simulation setup used to predict the EAC of noble gases with CNTs. The graphene setup is similar, with the source and sink being two parallel layers.

The interactions between carbon atoms are modeled with the adaptive intermolecular reactive empirical bond-order potential.[30] The interactions between gas atoms are modeled with 12−6 Lennard-Jones (LJ) potentials.[31,32] The LJ parameters for carbon−gas interaction are derived from the mixing rules $\sigma_{ij} = (\sigma_{ii} + \sigma_{jj})/2$ and $\varepsilon_{ij} = (\varepsilon_{ii}\varepsilon_{jj})^{1/2}$. All LJ parameters are provided in Table 1. The LJ interactions are truncated and shifted at a cutoff distance of 1 nm.

Table 1. Lennard-Jones Parameters Used To Model Gas−Gas and Gas−CNT Interactions[31,32]

atom type	atomic mass (amu)	σ (nm)	ε (meV)
C	12	0.34	2.4
He	4	0.256	0.88
Ne	20	0.275	3.07
Ar	40	0.34	10.61

The MD simulations were performed using LAMMPS[33] with a time step of 1 fs. The system was equilibrated at a temperature, T, of 300 K using the Nose−Hoover thermostat for 500 ps. The global thermostat was then turned off, a heat source (q = 640−4480 pW, depending on the gas species and the CNT diameters) was applied to the outer CNT (upper graphene layer), and a heat sink of the same magnitude was applied to the inner CNT (lower graphene layer), both through velocity rescaling. Steady state was reached after 10 ns, and data was collected for 20 to 40 ns. The simulations were designed so that the inner CNT (lower graphene layer) temperature was 300 K and the average gas temperature was 320 K. The outer CNT (upper graphene layer) temperature ranged from 320 to 340 K depending on the gas and inner CNT diameter.

To calculate the EAC, we tracked the gas atoms entering and departing a virtual cylinder surrounding the inner CNT with radius equal to the inner CNT radius plus the CNT−gas LJ cutoff distance. From the energy stream of gas atoms entering and departing this virtual cylinder, we calculated the EAC from eq 1. Because the system is at steady-state, we can also calculate the numerator of eq 1 from

$$E_{\text{incident}} - E_{\text{reflected}} = qt \tag{2}$$

where t is the data collection period. The predicted EACs from these two approaches are within their uncertainties. We find that the use of eq 2 leads to less uncertainty across multiple runs at the same conditions because only the incident gas atoms need to be tracked. For this reason, all reported results correspond to this approach.

PREDICTIONS

The EACs of He, Ne, and Ar as a function of CNT diameter are plotted in Figure 2. The EACs for graphene are 0.19 ± 0.01 (He), 0.43 ± 0.02 (Ne), and 0.93 ± 0.04 (Ar) and are plotted as dashed horizontal lines. The uncertainties correspond to the standard deviation of three simulations initialized with different velocities. Simulations of gas atoms interacting with multilayer graphene predict the same EAC as for the single-layer graphene, indicating that our results can be applied to multiwall CNTs. The EACs are unchanged with the addition of graphene layers because of (i) the low translational energies of the incident gas atoms, (ii) the weak van der Waals interaction between the gas atoms and the carbon atoms, and (iii) the long distance between the gas atoms and the second graphene layer. We note that this layer-independent EAC will likely not hold for higher translational energy gas atoms.[34] For the 0.68 nm CNT and Ar at a pressure of 2 atm, we predict the EAC to be 0.29, within the uncertainty of the prediction of 0.30 for a

dx.doi.org/10.1021/jp404153d | J. Phys. Chem. C 2013, 117, 18804−18808

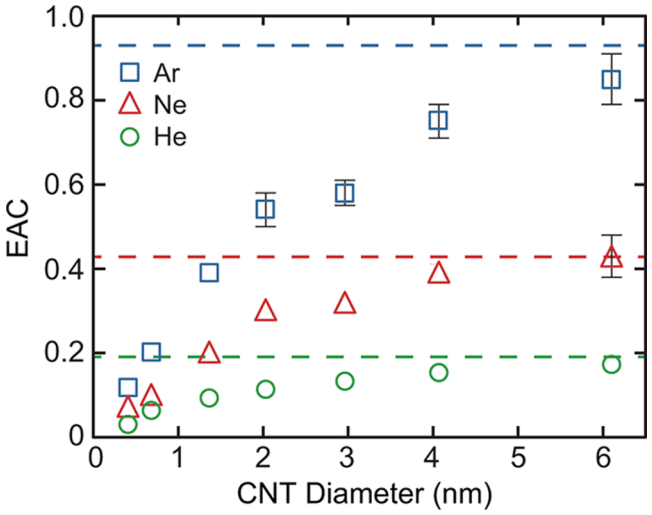

Figure 2. Diameter-dependence of noble gas–CNT EACs. The dashed lines are the EAC of each gas on graphene. The error bars correspond to the standard deviation from three independent simulations. If there are no error bars, the uncertainty is within the size of the data point. The CNT temperature is 300 K, and the gas temperature is 320 K.

pressure of 10 atm. This result suggests that the predicted EACs are independent of pressure.

The graphene EACs for He and Ne are comparable to MD-predicted values reported by Daun et al.[29] at a wall temperature of 3000 K and an incident gas temperature of 300 K (0.19 for He, 0.36 for Ne), while their EAC for Ar is lower, with a value of 0.46. When we repeated our Ar-graphene simulations using Daun et al.'s LJ parameters, we predict an EAC of 0.92, within the uncertainty of our original prediction. This result suggests that the differences between our data and Daun et al.'s may be due to the different wall temperature and/or the simulation methodology.

For a given CNT diameter, the EAC increases as the gas atomic mass increases. This trend is consistent with theoretical predictions[12] and previous MD modeling[14,29] and can be attributed to heavier gas atoms having a lower velocity and thus a longer interaction time with the CNT.

For a given gas, the EAC increases monotonically with CNT diameter and approaches the graphene value. By placing isolated CNTs in uniaxial tension, we predict that the Young's modulus decreases from 998 to 805 GPa as the diameter is increased from 0.41 to 6.10 nm. These very high moduli suggest that any softening of the surface stiffness as the diameter increases does not affect the EAC. To further explore the diameter trend, we calculated the potential energy surface of the gas–CNT (graphene) interaction for each of our systems by finely sampling points along the CNT unit cell at different distances from the surface. The results for Ar are plotted in Figure 3a. The depth of the gas–CNT potential well increases with increasing CNT diameter because less curvature leads to more and stronger interactions within the cutoff radius. The results for He and Ne are similar. This increase of EAC with increasing well depth is consistent with the predictions of Daun et al. for noble gases interacting with graphite and metal surfaces.[14]

We next normalized the CNT EACs by the graphene EAC for each gas. The results are plotted in Figure 3b versus the gas–CNT potential well depth normalized by that for

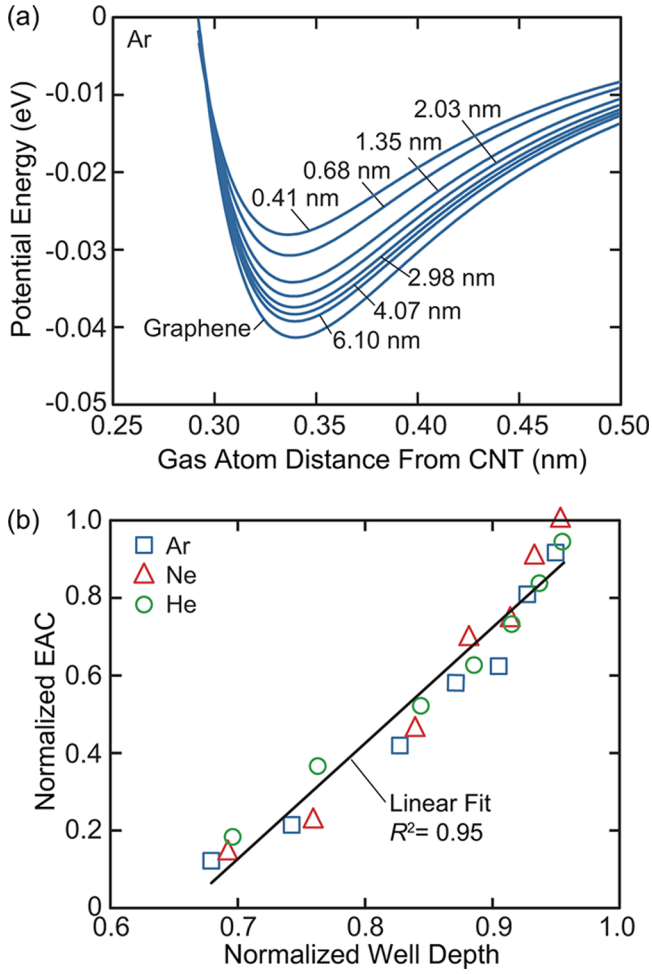

Figure 3. (a) Radial-dependence of the potential energy landscape experienced by an Ar atom on graphene and CNTs of different diameter. (b) The EAC data collapse when they are normalized by the corresponding graphene value and plotted versus the potential energy well depth on each CNT normalized by that for graphene. The data points are the same as those plotted in Figure 2.

graphene. The data for all gases and CNT diameters collapse to a linear trend, suggesting that the EAC is proportional to well depth and that there is a universal behavior for noble gas–CNT interactions. The collapse of the mass and diameter data is likely due to the link between increasing mass and increasing interaction strength for the noble gases (see Table 1). We note that our range of systems spans the CNT with the smallest known diameter [0.41 nm for a (3,3) chirality][35] to graphene, which is equivalent to a CNT with infinite curvature. Given the well depth and the EAC for graphene, one can therefore estimate the EAC for a CNT of any diameter. Further work is required to determine if this scaling law applies to noble gases with higher incident translational energies (i.e., higher temperatures).

The EAC can be used to predict the solid–gas thermal boundary conductance, h, from[20]

$$h = \frac{4k_B N\alpha}{2-\alpha} \tag{3}$$

where k_B is the Boltzmann constant and N is the gas collision rate on the solid surface per unit area, which can be obtained from the MD simulations. For He, Ne, and Ar on graphene, we

dx.doi.org/10.1021/jp404153d | J. Phys. Chem. C 2013, 117, 18804–18808

predict thermal boundary conductances of 0.44, 0.51, and 1.15 MW/m^2·K. These values are of the same order of magnitude as that for a Pt−Ar system modeled by Liang et al., also at a pressure near 10 atm.[15] The thermal boundary conductance should scale linearly to lower pressures because the EACs are pressure-independent and the collision rate is directly proportional to pressure.[20] The thermal boundary conductances between noble gases and graphene at atmospheric conditions should therefore be of order 0.1 MW/m^2·K. This value is the same as that estimated by Hu et al. using MD simulations for a (10,10) CNT in air at a pressure of 1 atm.[36]

The gas Kapitza length, defined as the ratio of the bulk gas thermal conductivity to the thermal boundary conductance, indicates the gas thickness that has the same thermal resistance of the boundary. Using the Green−Kubo method in equilibrium MD simulations,[37] we predict the thermal conductivity of Ar at a temperature of 320 K and a pressure of 1 atm to be 0.015 W/m·K. The Ar-graphene Kapitza length at these conditions will therefore be of order 100 nm.

SUMMARY

We used a nonequilibrium steady-state MD method to predict EACs between noble gases and graphitic surfaces of different curvature. The collapse of the EAC data shown in Figure 3(b) suggests universal behavior that may exist for other gases. The predicted EACs and thermal boundary conductances will be useful in the design and analysis of CNT- and graphene-based devices that interact with a gas environment.

AUTHOR INFORMATION

Corresponding Author

*E-mail: mcgaughey@cmu.edu.

Notes

The authors declare no competing financial interest.

ACKNOWLEDGMENTS

This work was supported by NSF award CBET0933510 (L.H., A.J.H.M.) and a Harrington Faculty Fellowship at The University of Texas at Austin (A.J.H.M.). We thank Jason M. Larkin (Carnegie Mellon University) for performing the Green-Kubo thermal conductivity predictions. We thank Kyle J. Daun (University of Waterloo) for helpful discussions.

REFERENCES

(1) Li, J.; Lu, Y.; Ye, Q.; Cinke, M.; Han, J.; Meyyappan, M. Carbon Nanotube Sensors for Gas and Organic Vapor Detection. *Nano Lett.* **2003**, *3*, 929−933.

(2) Modi, A.; Koratkar, N.; Lass, E.; Wei, B.; Ajayan, P. M. Miniaturized Gas Ionization Sensors using Carbon Nanotubes. *Nature* **2003**, *424*, 171−174.

(3) Kinefuchi, I.; Shiomi, J.; Takagi, S.; Maruyama, S.; Matsumoto, Y. Gas−Surface Energy Exchange in Collisions of Helium Atoms with Aligned Single-Walled Carbon Nanotube Arrays. *J. Phys. Chem. C* **2013**, *117*, 14254−14260.

(4) Dillon, A. C.; Jones, K. M.; Bekkedahl, T. A.; Kiang, C. H.; Bethune, D. S.; Heben, M. J. Storage of Hydrogen in Single-walled Carbon Nanotubes. *Nature* **1997**, *386*, 377−379.

(5) Liu, C.; Fan, Y. Y.; Liu, M.; Cong, H. T.; Cheng, H. M.; Dresselhaus, M. S. Hydrogen Storage in Single-Walled Carbon Nanotubes at Room Temperature. *Science* **1999**, *286*, 1127−1129.

(6) Zhu, W.; Bower, C.; Zhou, O.; Kochanski, G.; Jin, S. Large Current Density from Carbon Nanotube Field Emitters. *Appl. Phys. Lett.* **1999**, *75*, 873−875.

(7) Murakami, H.; Hirakawa, M.; Tanaka, C.; Yamakawa, H. Field Emission from Well-aligned, Patterned, Carbon Nanotube Emitters. *Appl. Phys. Lett.* **2000**, *76*, 1776−1778.

(8) Hsu, I.-K.; Pettes, M. T.; Aykol, M.; Shi, L.; Cronin, S. B. The Effect of Gas Environment on Electrical Heating in Suspended Carbon Nanotubes. *J. Appl. Phys.* **2010**, *108*, 084307.

(9) Jeans, S. J. *An Introduction to the Kinetic Theory of Gases*; Cambridge University Press: Cambridge, 1940.

(10) Chen, H.; Johnson, J. K.; Sholl, D. S. Transport Diffusion of Gases Is Rapid in Flexible Carbon Nanotubes. *J. Phys. Chem. B* **2006**, *110*, 1971−1975.

(11) Arya, G.; Chang, H.; Maginn, E. J. Molecular Simulations of Knudsen Wall-slip: Effect of all Morphology. *Mol. Simul.* **2003**, *29*, 697−709.

(12) Goodman, F. O. Thermal Accommodation Coefficients. *J. Phys. Chem.* **1980**, *84*, 1431−1436.

(13) Barker, J. A.; Auerbach, D. J. Gas-surface Interactions and Dynamics: Thermal Energy Atomic and Molecular Beam Studies. *Surf. Sci. Rep.* **1985**, *4*, 1−99.

(14) Daun, K.; Sipkens, T.; Titantah, J.; Karttunen, M. Thermal Accommodation Coefficients for Laser-induced Incandescence Sizing of Metal Nanoparticles in Monatomic Gases. *Appl. Phys. B: Laser Opt.* **2013**, 1−12.

(15) Liang, Z.; Evans, W.; Keblinski, P. Equilibrium and Non-equilibrium Molecular Dynamics Simulations of Thermal Conductance at Solid-gas Interfaces. *Phys. Rev. E* **2013**, *87*, 022119.

(16) Day, B. S.; Shuler, S. F.; Ducre, A.; Morris, J. R. The Dynamics of Gas-surface Energy Exchange in Collisions of Ar Atoms with Omega-functionalized Self-assembled Monolayers. *J. Chem. Phys.* **2003**, *119*, 8084−8096.

(17) Bennett, M. E.; Alexander, W. A.; Lu, J. W.; Troya, D.; Morris, J. R. Collisions of Polar and Nonpolar Gases with Hydrogen Bonding and Hydrocarbon Self-Assembled Monolayers. *J. Phys. Chem. C* **2008**, *112*, 17272−17280.

(18) Lu, J. W.; Alexander, W. A.; Morris, J. R. Gas-surface Energy Exchange and Thermal Accommodation of CO2 and Ar in Collisions with Methyl, Hydroxyl, and Perfluorinated Self-assembled Monolayers. *Phys. Chem. Chem. Phys.* **2010**, *12*, 12533−12543.

(19) Liang, Z.; Evans, W.; Desai, T.; Keblinski, P. Improvement of Heat Transfer Efficiency at Solid-gas Interfaces by Self-assembled Monolayers. *Appl. Phys. Lett.* **2013**, *102*, 061907.

(20) Goodman, F. O.; Wachman, H. Y. *Dynamics of Gas-Surface Scattering*; Academic Press: New York, 1976.

(21) Cahill, D. G.; Ford, W. K.; Goodson, K. E.; Mahan, G. D.; Majumdar, A.; Maris, H. J.; Merlin, R.; Phillpot, S. R. Nanoscale Thermal Transport. *J. Appl. Phys.* **2003**, *93*, 793−818.

(22) Schiffres, S. N.; Kim, K. H.; Hu, L.; McGaughey, A. J. H.; Islam, M. F.; Malen, J. A. Gas Diffusion, Energy Transport, and Thermal Accommodation in Single-Walled Carbon Nanotube Aerogels. *Adv. Funct. Mater.* **2012**, *22*, 5251−5258.

(23) Chirita, V.; Pailthorpe, B.; Collins, R. Non-equilibrium Energy and Momentum Accommodation Coefficients of Ar Atoms Scattered from Ni(001) in the Thermal Regime: A Molecular Dynamics Study. *Nucl. Instrum. Methods Phys. Res., Sect. B* **1997**, *129*, 465−473.

(24) Sun, J.; Li, Z.-X. Molecular Dynamics Simulations of Energy Accommodation Coefficients for Gas Flows in Nano-channels. *Mol. Simul.* **2009**, *35*, 228−233.

(25) Någård, M. B. N.; Andersson, P. U.; Marković, N.; Pettersson, J. B. C. Scattering and Trapping Dynamics of Gas−Surface Interactions: Theory and Experiments for the Xe-graphite System. *J. Chem. Phys.* **1998**, *109*, 10339−10349.

(26) Bolton, K.; Rosen, A. Computational Studies of Gas-carbon Nanotube Collision Dynamics. *Phys. Chem. Chem. Phys.* **2002**, *4*, 4481−4488.

(27) Bolton, K.; Gustavsson, S. Energy Transfer Mechanisms in Gas-carbon Nanotube Collisions. *Chem. Phys.* **2003**, *291*, 161−170.

(28) Kovalev, V.; Yakunchikov, A. Accommodation Coefficients for Molecular Hydrogen on a Graphite Surface. *Fluid Dynamics* **2010**, *45*, 975−981.

(29) Daun, K.; Smallwood, G.; Liu, F. Molecular Dynamics Simulations of Translational Thermal Accommodation Coefficients for Time-resolved LII. *Appl. Phys. B: Laser Opt.* **2009**, *94*, 39−49.
(30) Stuart, S. J.; Tutein, A. B.; Harrison, J. A. A Reactive Potential for Hydrocarbons with Intermolecular Interactions. *J. Chem. Phys.* **2000**, *112*, 6472−6486.
(31) Ackerman, D. M.; Skoulidas, A. I.; Sholl, D. S.; Johnson, J. K. Diffusivities of Ar and Ne in Carbon Nanotubes. *Mol. Simul.* **2003**, *29*, 677−684.
(32) Tuzun, R. E.; Noid, D. W.; Sumpter, B. G.; Merkle, R. C. Dynamics of Fluid Flow Inside Carbon Nanotubes. *Nanotechnology* **1996**, *7*, 241.
(33) Plimpton, S. Fast Parallel Algorithms for Short-Range Molecular Dynamics. *J. Comput. Phys.* **1995**, *117*, 1−19.
(34) Watanabe, Y.; Yamaguchi, H.; Hashinokuchi, M.; Sawabe, K.; Maruyama, S.; Matsumoto, Y.; Shobatake, K. Energy Transfer in Hyperthermal Xe-graphite Surface Scattering. *Eur. Phys. J., D* **2006**, *38*, 103−109.
(35) Guan, L.; Suenaga, K.; Iijima, S. Smallest Carbon Nanotube Assigned with Atomic Resolution Accuracy. *Nano Lett.* **2008**, *8*, 459−462. PMID: 18186659.
(36) Hu, M.; Shenogin, S.; Keblinski, P.; Raravikar, N. Thermal Energy Exchange Between Carbon Nanotube and Air. *Appl. Phys. Lett.* **2007**, *90*, 231905.
(37) McQuarrie, D. A. *Statistical Mechanics*; University Science Books: Sausalito, 2000.